Table of Contents

For the first time, it has been investigated by XAS the interaction between exfoliated black phosphorus (bP) and Pd NPs grown on it. A very short Pd-P distance was measured which demonstrates the presence of a covalent bond. This infers high structural stability to the nanohybrid and, more importantly, it is created a synergy which is responsible for the high chemoselectivity observed in the hydrogenation of chloro-nitroarenes to the corresponding chloro-anilines.

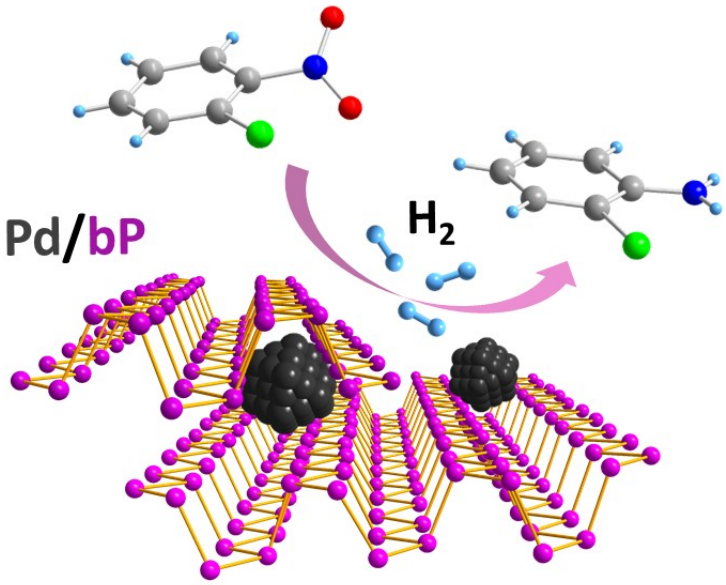

ABSTRACT

The burgeoning interest in 2D black phosphorus (bP) contributes to expand its applications in countless fields. In the present study, 2D bP is used as a support for homogeneously dispersed palladium nanoparticles directly grown on it by a wet chemical process. EELS-STEM analysis evidences a strong interaction between palladium and P atoms of bP nanosheets. A quantitative evaluation of this interaction comes from XAS measurements that find out a very short Pd-P distance of 2.26 Å proving for the first time the existence of an unprecedented Pd-P coordination bond of covalent nature. Additionally, the average Pd-P coordination number of about 1.7 reveals that bP acts as a polydentate phosphine ligand towards the surface Pd atoms of the nanoparticles, thus preventing their agglomeration and inferring structural stability. These unique properties result in a superior performance in the catalytic hydrogenation of chloro-nitroarenes to chloroaniline, where a higher chemoselectivity in comparison to other heterogeneous catalyst based on palladium has been observed.

Black Phosphorus/Palladium Nanohybrid: Unraveling the Nature of P-Pd Interaction and Application in Selective Hydrogenation

Matteo Vanni,[a,h] Manuel Serrano-Ruiz,[a] Francesca Telesio,[b] Stefan Heun,[b] Martina Banchelli,[c] Paolo Matteini,[c] Antonio Massilimiliano Mio,[d] Giuseppe Nicotra,[d] Corrado Spinella,[d] Stefano Caporali,[e] Andrea Giaccherini,[f] Francesco d'Acapito,[g] Maria Caporali,[a,*] Maurizio Peruzzini[a,*]

[a]CNR-ICCOM, Via Madonna del Piano10, 50019 Sesto Fiorentino, Italy

[b]NEST Istituto Nanoscienze-CNR and Scuola Normale Superiore, Piazza S. Silvestro 12, 56127 Pisa, Italy

[c]CNR-IFAC, Via Madonna del Piano10, 50019 Sesto Fiorentino, Italy

[d]CNR-IMM Istituto per la Microelettronica e Microsistemi, VIII strada 5, I-95121 Catania, Italy.

[e]Department of Industrial Engineering, University of Florence, Via di S. Marta 3, Florence, 50139, Italy

[f]Department of Earth Sciences, University of Florence, Via La Pira 4, Firenze, 50121, Italy

[g]CNR-IOM-OGG, c/o European Synchrotron Radiation Facility - LISA CRG, Grenoble, France.

[h]Department of Biotechnology, Chemistry and Pharmacy, University of Siena, 53100 Siena, Italy

With the advent of molybdenum disulfide and black phosphorus (bP) as emerging 2D materials which have embraced the common interests of physicists, chemists and material scientists, the post-graphene era just started. The peculiar physical properties of black phosphorus are serendipitously in between those of graphene and transition-metal dichalcogenides, as the direct tunable energy band gap (0.3 eV in the bulk, 1.8 eV for the monolayer) and the high carrier mobility at room temperature (1000 $cm^2V^{-1}s^{-1}$), desirable for high-performance mechanically flexible field-effect transistors (FET) devices.[1] bP has a unique puckered honeycomb structure derived from the sp^3 hybridization of phosphorus atoms that in turn gives rise to strong in-plane anisotropy of many physical properties such as heat and electron flow which varies according to the armchair and zig-zag direction, respectively.[2] Furthermore, the presence of a lone pair on each P-atom opens the way to several surface modifications. Indeed, several studies have addressed the chemical functionalization of bP, either covalent[3] or not,[4] aiming to improve the processability of the material and the ambient stability,[2-5] which is the Achille's heel of bP. A growing field is the study of bP as support for metal and metal phosphide nanoparticles to trigger applications in catalysis. Taking advantage of its intrinsic property of being a semiconductor, few-layer bP has been tested in photocatalytic processes, either alone or combined with a metal as co-catalyst, in hydrogen evolution reaction (HER),[6] water-splitting[7] and photodegradation of organic pollutants.[8,9] Other catalytic applications were shown for various M NPs/bP nanohybrids where M = Co,[10] Ni,[11] Pt.[12] Recently, Pd NPs were anchored on anatase TiO_2-bP hybrid for ethanol electrooxidation.[13] Nevertheless, up to now there is no experimental study on the fundamental interaction between metal nanoparticles and P atoms of bP. Our current work represents the first important step on the elucidation of the nature of this interaction and shows how the interplay between bare palladium nanoparticles and exfoliated black phosphorus makes Pd/bP a highly selective heterogeneous catalyst.

The synthesis of Pd/bP was carried out in solution by direct growth of Pd NPs on exfoliated bP nanosheets obtained by ultrasonication,[14] see ESI. The morphology of the new 2D material was first studied by SEM which shows that Pd NPs are embedded in the bP nanosheets, see Figure 1a. Inspection by TEM, high angle annular dark field scanning transmission electron microscopy (HAADF STEM) and energy dispersive X-ray spectroscopy (EDS) confirmed the formation of nearly spherical palladium nanoparticles homogeneously distributed on the bP nanosheets and with a relative narrow size distribution centered at 3.1±0.8 nm, see Figure 1b-c-d below. Atomic force microscopy (AFM) revealed the presence of both thin and thick flakes with mean size around 600 nm and thickness going from 5 nm to 200 nm (Figure 1e and S4).

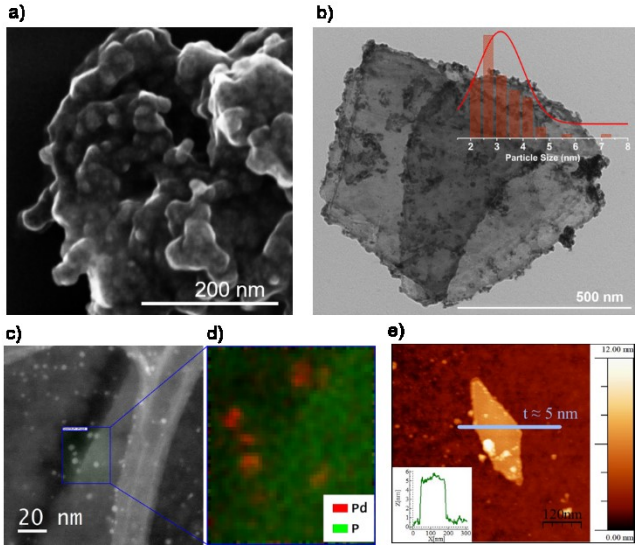

Figure 1. Structural characterization of Pd/bP. a) SEM image of Pd/bP. b) TEM image of Pd/bP and relative size distribution. Scale bar: 500 nm. c) High resolution HAADF STEM image of Pd/bP on a lacey carbon grid. Pd-rich areas can be clearly distinguished for the higher Z-contrast (brighter areas). The blue ROI indicates the region in which the EDS SI (spectrum imaging) was performed. (d)

EDS elemental mapping of the selected area on Pd/bP obtained integrating the signals from the Pd L-lines and the P K-lines. e) AFM image of a Pd/bP flake on Si/SiO_2. The line corresponds to the cross-sectional profile shown as an inset. The flake thickness is approximately 5 nm.

The nanohybrid Pd/bP was characterized by powder X-ray diffraction (PXRD) which confirms the phase purity of the 2D material and shows strong preferential orientation along the (0k0) direction, with three most intense peaks at 2θ = 16.8°, 34.2° and 52.2° assigned respectively to the (020), (040) and (060) planes of orthorhombic black phosphorus, see Figure 2a. This is also characteristic of the pristine material suggesting that its crystalline structure is retained upon functionalization with Pd NPs. A very broad peak around 2θ = 39.5° assigned to the (111) planes of Pd confirms the presence of a nanosized fcc phase of the metal.

It is well established[15] that the three Raman peaks of bP at 357.8, 431.5 and 459.2 cm^{-1}, corresponding to the Raman active phonon mode A^1_g, B^2_g and A^2_g respectively, are thickness dependent and may undergo a frequency shift with varying flake thickness. Given the thickness polydispersity of bP prepared by sonochemical exfoliation, micro-Raman spectra were collected for a large set of flakes in order to take into account the broad range of thickness. As shown in Figure 2b, Raman spectrum of Pd/bP displays the three peaks characteristic of the orthorombic phase of bP observed above by XRD, however no significant frequency shift was detected compared to pristine bP. Figure S5 shows a detailed statistics for the A^1_g, B^2_g and A^2_g Raman modes of pristine bP and Pd/bP.

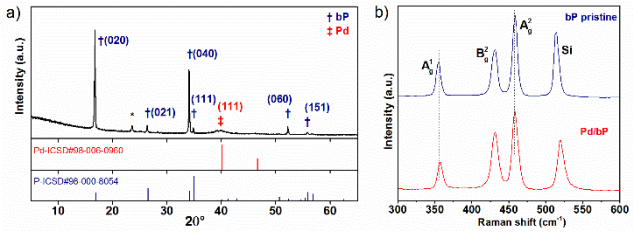

Figure 2. a) XRD spectrum of Pd/bP. b) Comparison of Raman spectra collected on pristine bP (red) and Pd/bP (blue). Each spectrum has been obtained combining the data from 15 different flakes.

EELS (Electron Energy Loss Spectroscopy) is an important tool to gain information on the chemical shifts of core-level states, as well as on the fine structure of the unoccupied valence-band states, thus we performed a comparative EELS analysis between bP (simulated[16] and measured) and Pd/bP measured by HAADF-STEM-SI, see Figure 3. An appreciable difference in the P_L-edge is observed at around 137 eV for Pd/bP that reveals a modification of the electronic structure of bP which can be interpreted as the result of a strong interaction between P atoms of bP and Pd NPs.

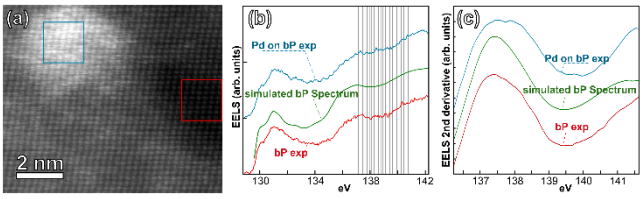

Figure 3. (a) HAADF-STEM-SI of Pd/bP acquired along the [101] zone axis, at the P L edge. (b) EELS spectra: red curve, experimental bP, obtained integrating the EELS-SI (spectrum imaging) along the red box in (a); green curve: simulated bP[16]; blue curve: experimental Pd/bP, obtained integrating the EELS-SI along the blue box in (a). (c) second derivative plots of the three EELS spectra within the region highlighted in (b).

The chemical states of the Pd NPs were determined by the Pd 3d core-level XPS spectrum (Figure 4a), which is fitted by the use of two doublets due to spin-orbit couplings. The components at binding energy B.E. = 335.8 eV (Pd $3d_{5/2}$) and at B.E. = 341.0 eV (Pd $3d_{3/2}$) accounts for bulk metallic palladium.[17a] The smaller doublet at B.E. = 338.1 eV and B.E. = 343.5 eV is attributable to an electro-depleted palladium specie, probably with an oxidation state +2. The presence of PdO can be ruled out being absent the peaks with corresponding B.E. values,[17b] thus the signal at higher binding energy can be explained as the result of a partial valence orbital overlap between surface Pd atoms and bP nanosheets. This is consistent with the presence of Pd-P bonds, as deduced from the EELS measurements. The presence of a layer of electron-depleted palladium atoms on the surface of Pd NPs, which strongly interacts with P-atoms, has been already observed[18] in the study of Pd NPs capped with the phosphine ligand PTA (PTA = 1,3,5-triaza-7-phophaadamantane), which indeed show a comparable XPS spectrum.

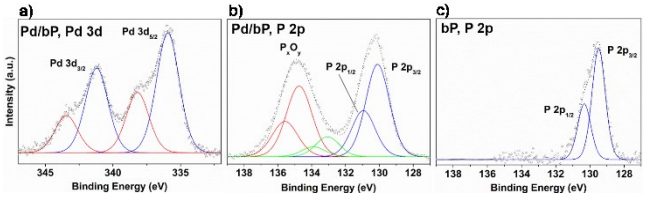

Figure 4. a) Pd 3d core level XPS spectrum of Pd/bP. Metallic and electron-depleted palladium doublets are depicted by blue and red lines, respectively. b) P 2p core level XPS spectrum of Pd/bP, the fitting here requires the use of three different components as discussed in the text. c) P 2p core level XPS spectrum of pristine bP.

The deconvolution of P 2p core level spectrum for pristine bP shows the characteristic doublet representing the P $2p_{3/2}$ and P $2p_{1/2}$ peaks located at 129.7 eV and 130.6 eV, typical of elemental phosphorus, see Figure 4c. Intriguingly, P 2p core level spectrum of Pd/bP results much more complex requiring the use of at least three components. Alongside the doublet attributable to elemental phosphorus (two peaks at B.E.= 130 eV and B.E. = 131 eV), components at higher B.E. values are present as well, see Figure 4b, that can be interpreted as due to phosphorus in different chemical environments. The doublet at intermediate B.E. values (green line fitting in figure 4b) is likely due to P-Pd bonds. The large doublet characterized by the highest binding energy (red line fitting in figure 4b) accounts for the presence of phosphorus oxides species such as P-OH, P=O and P-O-P on the surface of bP sheets.[19] Since peaks at lower BE values characteristic of P having a phosphide nature (128.6 eV)[20] are absent, the presence of phosphides as Pd_xP_y can be excluded.

To the best of our knowledge, the nature of the interaction between metal nanoparticles and bP has been so far approached only by theoretical calculations. For instance, the nanohybrid Ag/bP has been described as stabilized by covalent bonds at the Ag/bP interface by means of DFT calculations[8] but up to now

no experimental investigations have been carried out. To unravel the nature of the Pd-P interaction, X-ray absorption spectroscopy (XAS) measurements were performed on Pd/bP and the following compounds were taken as standards: Pd NPs capped with the phosphine ligand PTA and labelled as Pd@PTA,[18] palladium phosphide nanoparticles PdP_2 NPs,[21] Pd NPs supported on carbon Pd/C[22] and Pd metal foil, see Table S1.

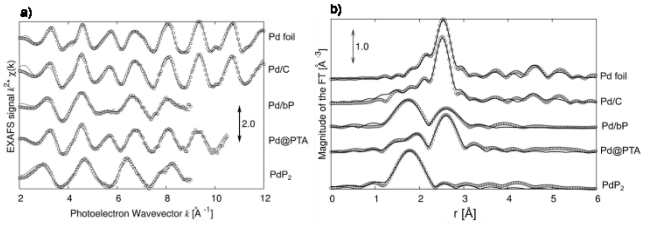

Figure 5. a) EXAFS data at the Pd-K edge; b) the corresponding Fourier transforms. Dots are experimental data while continuous lines are the calculated best-fit data. *(cambiare con quelle che ti ho inviato col mail)*

In Fig. 5, the raw EXAFS spectra and the corresponding Fourier Transforms; these show clearly the presence of a peak just below 2 Å in the sample Pd/bP. This peak is at higher values if compared with PdO suggesting the presence of a ligand different form Oxygen that could be attributed to Pd-P. A comparison with the TFs shows a position near to PdP_2 whereas the quantitative data fit resulted to be possible only with P ligands as tentatives with O lead to unphysical results. This is obvious because the two atoms have substantially different backscattering functions and appreciably different bond length values (R_{PdO}=2.00 Å, R_{PdP}=2.26 Å, see SI). For A second peak just below 3 Å can be inferred to Pd-Pd bonds, being present both in Pd metal foil, Pd/C and Pd@PTA. This means that Pd atoms are involved in two different bonds: Pd-Pd and Pd-P, the former arising from the bonds with inner metal atoms of the nanoparticle, the latter from an interaction between the surface Pd atoms and P atoms of bP. The precise value of bond lengths can be obtained from these data by fittings and are shown in Table S2. Noteworthy, the short Pd-P distance, R_{PdP} = 2.26(3) Å found in Pd/bP points out that the latter is a very strong interaction. As a comparison, the phosphide PdP_2 has longer bonds, R_{PdP} = 2.32(2) Å, as measured by us and according to literature,[23] while PdP_3 has[24] R_{PdP} = 2.235 Å which is close to Pd/bP, see Table S2, but the presence of phosphide can be for sure excluded in our sample on the basis of XPS measurements previously discussed. Remarkably, Pd@PTA exhibits R_{PdP} = 2.25 Å, which is consistent with the coordination bond distance Pd-P of 2.203(3) Å measured[25] in the X-ray structure of the complex cation $[Pd(PTAH)_4]^{4+}$, and it is almost the same value measured in Pd/bP. This reveals the Pd-P interaction in Pd/bP can be seen as a coordination bond of covalent nature and closely resembles the one exhisting in Pd@PTA: the P atoms of the bP nanosheets surround Pd NPs acting similarly to the molecular phosphine ligand PTA towards Pd NPs. This folding agrees well with the morphology observed by SEM, see Figure1a, and also explains the stacking of the flakes, observed by AFM, see Figure S4. The observed average Pd-P coordination number CNs=1.7(6) in our sample, see ESI for details, fairly corroborates this picture.

To the best of our knowledge, this is the first experimental demonstration that bP nanosheets may act as a polydentate phosphorus ligand towards metal nanoparticles via coordination bonds. This strong interaction, confers a stabilization to Pd NPs preventing their agglomeration and makes Pd/bP a good candidate for catalysis. Intrigued by these results, the chemical process studied was the reduction of chloro-nitroarenes to the corresponding chloroanilines, see Scheme 1. The latter are high valuable intermediates for the manufacture of many agrochemicals, pharmaceuticals, polymers and dyes.[26] Since traditional methods employing stoichiometric reducing agents have drawbacks for both economic and environmental issues, efforts have been devoted to replace them with hydrogen gas. However, many tested catalysts are severely affected by undesired dehalogenation due to the C–Cl hydrogenolysis, (see Figure S6), thus finding a catalyst able to efficiently carry out a chemoselective reduction of nitroarenes remains a challenge.

Scheme 1. Hydrogenation of chloro-nitroarenes to chloroanilines.

Satisfyingly, Pd/bP showed very high chemoselectivity in the reduction of both *ortho* and *meta*-chloronitrobenzene, reaching 97.3% of selectivity toward the chloroaniline at 99.5% conversion for the *ortho* isomer, see Table S3, overwhelming other heterogeneous catalysts based on Pd NPs[27] that are affected by dehalogenation. As a comparison, Pd NPs with similar average size were grown on a highly porous carbon, ketjen black, see ESI, and at complete conversion the chemoselectivity dropped down to 78.1% as shown in Table S3. Undoubtedly, bP plays a key role since it behaves as a ligand towards Pd NPs, a unique feature that a carbon-based support cannot supply. Additionally, it is relevant that the TOFs are almost the same using as a support either bP or ketjen black, even if the latter is characterized by a very high surface area (1400 m^2/g).

Catalyst reuse was also tested, showing the selectivity was maintained unaltered for six consecutive runs, only a small decrease of the conversion was observed, see Figure S7. In agreement with this, TEM investigation on Pd/bP recovered after the catalytic runs, confirmed the morphology was preserved, being the average size of Pd NPs equal to 3.6±0.9 nm, see Figure S8, and the heterogeneous nature of our catalyst was proved as well with an independent test, see Table S4. Thus, the presence of Pd-P bonds prevents bP degradation and provides an excellent structural stability to our catalyst.

In summary, a new Pd/bP nanohybrid has been developed and for the first time, the intimate nature of the interaction between Pd NPs and bP nanosheets was elucidated by EXAFS. A very short Pd-P distance of 2.26(3) Å was disclosed, accounting for a coordinative bond of covalent nature between surface Pd atoms and P atoms. Moreover, the average Pd-P coordination number turned out to be 1.7 (6), which suggests bP acts as a polydentate phosphine ligand towards Pd NPs, stabilizing them toward agglomeration and preventing leaching of the metal in solution. Pd NPs are thus embedded between bP flakes yielding a new 0D-2D heterostructure. The latter was also investigated with other surface techniques, as XPS and EELS-STEM, all of them are consistent with the presence of Pd-P bonds. Finally, the synergy between Pd NPs and bP was successfully exploited in the reduction of chloro-nitroarenes to the corresponding chloro-anilines, showing a far superior chemoselectivity in

comparison to other heterogeneous catalysts based on palladium. Furthermore, Pd/bP was reused and maintained its efficiency after six consecutive runs, demonstrating an intrinsic stability that promises further applications in various fields.

ASSOCIATED CONTENT

Supporting Information. The Supporting Information is available free of charge on the ACS Publications website

AUTHOR INFORMATION

Corresponding Author

*(M.C.) E-mail: maria.caporali@iccom.cnr.it
ORCID M. Caporali: 0000-0001-6994-7313
*(M.P.) E-mail: maurizio.peruzzini@iccom.cnr.it
ORCID M. Peruzzini: 0000-0002-2708-3964

Notes

The authors declare no conflict of interest.

ACKNOWLEDGMENTS

Thanks are expressed to EC for funding the project PHOSFUN "Phosphorene functionalization: a new platform for advanced multifunctional materials" (ERC ADVANCED GRANT to M.P.). STEM-EELS analysis was performed at Beyond-Nano CNR-IMM, which is supported by the Italian Ministry of Education and Research (MIUR) under project Beyond-Nano (PON a3_00363).
The authors gratefully acknowledge for SEM and TEM images "Ce.M.E. – Centro Microscopie Elettroniche Laura Bonzi" in Sesto Fiorentino (Italy) financed by "Ente Cassa di Risparmio di Firenze" and through the projects "EnergyLab", POR FESR 2014-2020 and FELIX (Fotonica ed Elettronica Integrate per l'Industria, project code n. 6455). Finally, MIUR is kindly acknowledged for financial support through Project PRIN 2015 (grant number 20154X9ATP).

REFERENCES

(1) Li, L.; Yu, Y.; Ye, G.; Ge, Q.; Ou, X.; Wu, H.; Feng, D.; Chen, X. H.; Zhang, Y. Black Phosphorus Field-Effect Transistors. *Nature Nanotechnol.* **2014**, *9*, 372 – 377.

(2) Gusmão, R.; Sofer, Z.; Pumera, M. Black Phosphorus Rediscovered: from Bulk Material to Monolayers. *Angew. Chem. Int. Ed.* **2017**, *56*, 8052 – 8072.

(3) a) Sofer, Z.; Luxa, J.; Bouša, D.; Sedmidubský, D.; Lazar, P.; Hartman, T.; Hardtdegen, H.; Pumera, M. The Covalent Functionalization of Layered Black Phosphorus by Nucleophilic Reagents. *Angew. Chem. Int. Ed.* **2017**, *56*, 9891 – 9896; b) van Druenen, M.; Davitt, F.; Collins, T.; Glynn, C.; O'Dwyer, C.; Holmes, J. D.; Collins, G. Covalent Functionalization of Few-Layer Black Phosphorus using Iodonium Salts and Comparison to Diazonium Modified Black Phosphorus. *Chem. Mater.* **2018**, *30*, 4667− 4674.

(4) a) Abellán, G.; Neiss, C.; Lloret, V.; Wild, S.; Chacln-Torres, J. C.; Werbach, K.; Fedi, F.; Shiozawa, H.; Görling, A.; Peterlik, H.; Pichler, T.; Hauke, F.; Hirsch, A. Exploring the Formation of Black Phosphorus Intercalation Compounds with Alkali Metals. *Angew. Chem. Int. Ed.* **2017**, *56*, 15267 –15273; b) Korolkov, V. V.; Timokhin, I. G.; Haubrichs, R.; Smith, E. F.; Yang, L.; Yang, S.; Champness, N. R.; Schröder, M.; Beton, P. H. Supramolecular Networks Stabilise and Functionalise Black Phosphorus. *Nature Commun.* **2017**, *8*, 1385.

(5) Kuriakose, S.; Ahmed, T.; Balendhran, S.; Bansal, V.; Sriram, S.; Bhaskaran, M.; Walia, S. Black Phosphorus: Ambient Degradation and Strategies for Protection. *2D Mater.* **2018**, *5*, 032001.

(6) a) Zhu, M.; Kim, S.; Mao, L.; Fujitsuka, M.; Zhang, J.; Wang, X. Metal-Free Photocatalyst for H_2 Evolution in Visible to Near-Infrared Region: Black Phosphorus/Graphitic Carbon Nitride. *J. Am. Chem. Soc.* **2017**, *139*, 13234−13242.

(7) Zhu, M.; Sun, Z.; Fujitsuka, M.; Majima, T. Z-Scheme Photocatalytic Water Splitting on a 2D Heterostructure of Black Phosphorus/Bismuth Vanadate Using Visible Light. *Angew. Chem. Int. Ed.* **2018**, *57*, 2160 –2164.

(8) Lei, W.; Zhang, T.; Liu, P.; Rodriguez, J. A.; Liu, G.; Liu, M. Bandgap and Local Field-Dependent Photoactivity of Ag/Black Phosphorus Nanohybrid. *ACS Catal.* **2016**, *6*, 8009-8020.

(9) Yuan, Y.-J.; Yang, S.; Wang, P.; Yang, Y.; Li, Z.; Chen, D.; Yu, Z.-T.; Zoub, Z.-G. Bandgap-Tunable Black Phosphorus Quantum Dots: Visible-Light-Active Photocatalysts. *Chem. Commun.* **2018**, *54*, 960-963.

(10) Shi, F.; Geng, Z.; Huang, K.; Liang, Q.; Zhang, Y.; Sun, Y.; Cao, J.; Feng, S. Cobalt Nanoparticles/Black Phosphorus Nanosheets: An Efficient Catalyst for Electrochemical Oxygen Evolution. *Adv. Sci.* **2018**, *5*, 1800575.

(11) Caporali, M.; Serrano-Ruiz, M.; Telesio, F.; Heun, S.; Nicotra, G.; Spinella, C.; Peruzzini, M. Decoration of Exfoliated Black Phosphorus with Nickel Nanoparticles and its Application in Catalysis. *Chem. Commun.* **2017**, *53*, 10946-10949.

(12) Bai, L.; Wang, X.; Tang, S.; Kang, Y.; Wang, J.; Yu, Y.; Zhou, Z.-K.; Ma, C.; Zhang, X.; Jiang, J.; Chu, P. K.; Yu, X.-F. Black Phosphorus/Platinum Heterostructure: A Highly Efficient Photocatalyst for Solar-Driven Chemical Reactions. *Adv. Mater.* **2018**, 1803641.

(13) Wu, T.; Fan, J.; Li, Q.; Shi, P.; Xu, Q.; Min, Y. Palladium Nanoparticles Anchored on Anatase Titanium Dioxide-Black Phosphorus Hybrids with Heterointerfaces: Highly Electroactive and Durable Catalysts for Ethanol Electrooxidation. *Adv. Energy Mater.* **2018**, *8*, 1701799.

(14) Serrano-Ruiz, M.; Caporali, M.; Ienco, A.; Piazza, V.; Heun, S.; Peruzzini, M. The Role of Water in the Preparation and Stabilization of High-Quality Phosphorene Flakes. *Adv. Mater. Interfaces*, **2016**, *3*, 1500441.

(15) Ribeiro, H. B.; Pimenta, M. A.; de Matos, C. J. S. Raman Spectroscopy in Black Phosphorus. J. Raman Spectrosc. 2018, 49, 76-90.

(16) Nicotra, G.; Politano, A.; Mio, A.M.; Deretzis, I.; Hu, J.; Mao, Z. Q.; Wei, J.; La Magna, A.; Spinella, C. Absorption Edges of Black Phosphorus: A Comparative Analysis. *Phys. Status Solidi B* **2016**, *253*, 2509-2514.

(17) a) Militello, M. C.; Simko, S. J. Elemental Palladium by XPS. *Surface Science Spectra* **1994**, *3*, 387; b) ibidem. Palladium Oxide by XPS. *Surface Science Spectra* **1994**, *3*, 395.

(18) Caporali, M.; Guerriero, A.; Ienco, A.; Caporali, S.; Peruzzini, M.; Gonsalvi, L. Water-Soluble, 1,3,5-Triaza-7-phosphaadamantane-Stabilized Palladium Nanoparticles and their Application in Biphasic Catalytic Hydrogenations at Room Temperature. *Chem. Cat. Chem.* **2013**, *5*, 2517 – 2526.

(19) a) Kuntz, K. L.; Wells, R. A.; Hu, J.; Yang, T.; Dong, B.; Guo, H.; Woomer, A. H.; Druffel, D. L.; Alabanza, A.; Tomanek, D.; Warren, S. C. Control of Surface and Edge Oxidation on Phosphorene. *ACS Appl. Mater. Interfaces* **2017**, *9*, 9126-9135.

(20) Wang, J.; Liu, D.; Huang, H.; Yang, N.; Yu, B.; Wen, M.; Wang, X.; Chu, P. K.; Yu, X.-F. In-Plane Black Phosphorus/Dicobalt Phosphide Heterostructure for Efficient Electrocatalysis. *Angew. Chem. Int. Ed*. **2018**, *57*, 2600-2604.

(21) Carenco, S.; Hu, Y.; Florea, I.; Ersen, O.; Boissière, C.; Sanchez, C.; Mezailles, N. Structural Transitions at the Nanoscale: the Example of Palladium Phosphides Synthesized from White Phosphorus. *Dalton Trans.* **2013**, *42*, 12667-12674.

(22) Miller, H. A.; Lavacchi, A.;Vizza, F. ; Marelli, M. ;Di Benedetto, F. ; D'Acapito, F. ; Paska, Y. ; Page, M. ; Dekel, D.R. A Pd/C-CeO2 Anode Catalyst for High-Performance Platinum-Free Anion Exchange Membrane Fuel Cells. *Angew. Chem. Int. Ed.* **2016**, *55*, 6004-6007.

(23) Zachariasen, W. H. The Crystal Structure of Palladium Diphosphide. *Acta Cryst.* **1963**, *16*, 1253.

(24) Rundqvist, S. Phosphides of the Platinum Metals. *Nature* **1960**, *185*, 31.

(25) Darensbourg, D. J.; Decuir, T. J.; Stafford, N. W.; Robertson, J. B.; Draper, J. D.; Reibenspies, J. H. Water-Soluble Organometallic Compounds. Synthesis, Spectral Properties, and Crystal Structures of

Complexes of 1,3,5-Triaza-7-phosphaadamantane with Group 10 Metals. *Inorg. Chem.* **1997**, *36*, 4218- 4226.

(26) Blaser, H.-U.; Steiner, H.; Studer, M. Selective Hydrogenation of Functionalized Nitroarenes: An Update. *Chem. Cat. Chem.* **2009**, *1*, 210-221.

(27) Costantino, F.; Nocchetti, M.; Bastianini, M.; Lavacchi, A.; Caporali, M.; Liguori, F. Robust Zirconium Phosphate−Phosphonate Nanosheets Containing Palladium Nanoparticles as Efficient Catalyst for Alkynes and Nitroarenes Hydrogenation Reactions. *ACS Appl. Nano Mat.* **2018**, *1*, 1750−1757.